Heliyon

ELSEVIER

Received:
29 October 2018
Revised:
6 February 2019
Accepted:
15 March 2019

Cite as: J. A. Rojas, L. A. Ardila-Rodríguez, M. F. Diniz, M. Gonçalves, B. Ribeiro, M. C. Rezende. Highly porous multiwalled carbon nanotube buckypaper using electrospun polyacrylonitrile nanofiber as a sacrificial material. Heliyon 5 (2019) e01386. doi: 10.1016/j.heliyon.2019.e01386

Highly porous multiwalled carbon nanotube buckypaper using electrospun polyacrylonitrile nanofiber as a sacrificial material

J. A. Rojas [a,*], L. A. Ardila-Rodríguez [b], M. F. Diniz [c], M. Gonçalves [a], B. Ribeiro [a], M. C. Rezende [a]

[a] *Federal University of São Paulo (UNIFESP), Institute of Science and Technology, São José dos Campos, SP, 12231280, Brazil*

[b] *Technological Institute of Aeronautics (ITA), Division of Fundamental Science, São José dos Campos, SP, 12228, Brazil*

[c] *Departamento de Ciência e Tecnologia Aeroespacial (DCTA), Instituto de Aeronáutica e Espaço (IAE), São José dos Campos, SP, 12228904, Brazil*

[*] Corresponding author.

E-mail address: jarojasc21@gmail.com (J.A. Rojas).

Abstract

Polyacrylonitrile (PAN) was solubilized in N,N-dimethyl formamide (DMF) and the electrospinning process has been employed to obtain PAN nanofibers (PF). Multiwalled carbon nanotubes (MWCNT) were dispersed with the aid of Triton X-100 surfactant and subsequently centrifugated. Buckypapers (BP/PF) were prepared by vacuum filtration procedure of MWCNT suspension supernatant stacking four PF layers over a nylon membrane. The PF removal was carried out by immersing the BP/PF system in DMF and removal periods of 10 and 30 min were evaluated. Scanning electron microscopy (SEM) has not shown any PAN residue in the MWCNT network resulting in highly porous BP. However, by Fourier transform infrared spectroscopy (FT-IR) a PAN band was found around of 2243 cm^{-1} corresponding to nitrile group (C≡N). Besides, PAN leftover was evidenced by thermogravimetric analysis (TGA), high-resolution transmission

https://doi.org/10.1016/j.heliyon.2019.e01386

electron microscopy (HR-TEM), electrical characterization through four-point probe, nitrogen adsorption at 77 K, and X-ray diffraction (XRD).

Keywords: Materials science, Nanotechnology

1. Introduction

Considered one of the most important materials due to their outstanding mechanical, electrical and thermal properties, carbon nanotubes (CNT) have been promoting a scientific revolution for almost three decades [1, 2, 3, 4]. The incorporation of CNT in different matrices and, consequently, the preparation of good polymer nanostructured composite depends basically on the adequate dispersion of this filler in the polymeric system. However, it is known that the low interaction of CNT with common solvents, their strong agglomerating tendency, the strong van der Waals interaction, and their high surface area cause a poor dispersion within polymer matrices which limits their practical applications [5, 6, 7, 8, 9].

In order to overcome the challenge related to CNT dispersion, several researches [10, 11, 12] have considered the use of a thin film of CNT, also known as Buckypaper (BP), which can be defined as a free-standing mat made of CNT. The BP can be prepared from a dispersion of randomly distributed CNT suspension that is filtrated through a membrane under vacuum conditions. As a result, the BP film forms a structure that can be considered as a CNT skeleton where the CNT are held together by the tube-tube junctions [6, 13, 14]. Several studies have been addressed to explore the potential applications of BP including polymer composites with high CNT loading (up to 60 wt%), supercapacitors, hydrogen storage materials, gas separators, electrodes, actuators, sensors, and artificial muscles [14, 15, 16, 17].

However, since the dispersion and inclusion of high amounts of CNT in polymer matrices have been solved, a new challenge arises related to impregnation of BP by polymer systems due to its low permeability. Lopes et al. [18] reported that due to small pore-size of the BP structure, it shows an intrinsic permeability value of 8−10 orders of magnitude lower than observed for conventional glass fibers based mats. As found in literature, several researches have been trying to improve the BP porosity. Liu et al. [19] studied the increase of BP porosity by using Polytetrafluoroethylene (PTFE) filtration membranes with pore diameters of 0.22, 0.8, and 1.2 μm. Kukovecz et al. [20] controlled the pore diameter of BP by using short multiwalled carbon nanotubes (MWCNT) (230 nm), and longer MWCNT (2 μm). Also, several authors have used sacrificial materials to improve the BP porosity. Dumée et al. [21] prepared a CNT suspension that was dispersed with polystyrene latex beads of 1 μm in order to fabricate the BP. At the end of the filtration process, the polystyrene latex beads were dissolved resulting in macrocavities in the BP morphology. Das et al. [22]

https://doi.org/10.1016/j.heliyon.2019.e01386

employed 200 nm diameter polystyrene nanospheres as sacrificial material promoting nanoholes throughout the CNT film.

In order to propose an alternative route to increase the low porosity presented by BP, this work introduces a new concept of high porous BP using electrospun polyacrylonitrile (PAN) nanofiber as sacrificial material. The electro-spinning technique is a cost-effective, simple, and fast process that allows to electrospun a wide range of polymers [23, 24, 25, 26, 27]. Also, the diameter of the fibers can vary from a few nanometers to a few micrometers and the fiber length can be several centimeters to several meters only by varying the polymer employed and the parameters of process, such as concentration of polymer solution, working distance, collector rotation, infusion rate, and electrical potential [27, 28, 29]. These variables allow the electrospinning technique to be a highly versatile process. The nano/micro fibers obtained can be used for various applications, such as cancer cell capture [30], air purification [31, 32], electrode material for supercapacitors [33], among other uses [34, 35].

The aim of the present work is to prepare a highly porous BP by the incorporation of electrospun PAN nanofibers (PF) as sacrificial material. PAN was chosen since it is the precursor of the carbon fibers and their incorporation into carbon nanotube BP could open a new research field. In this work, four PF layers were stacked over nylon membrane and MWCNT suspension was vacuum filtrated in order to obtain the carbon nanotube film. Afterwards, PF layers were dissolved in N,N-dimethyl formamide (DMF) at 60 °C under two different conditions. The samples were characterized by scanning electron microscopy (SEM), Fourier transform infrared spectroscopy (FT-IR), thermogravimetric analysis (TGA), X-ray diffraction (XRD), electrical resistance using a four-point probe, and high-resolution transmission electron microscopy (HRTEM). The surface area and the total pore volume were obtained by nitrogen adsorption/desorption technique at 77 K.

2. Materials and methods

2.1. Materials

In this research, multiwalled carbon nanotubes (MWCNT) synthesized by chemical vapor deposition technique (Purity >95%) were provided by Bayer Material Science, Germany, coded as Baytubes® C 150 P. The range of outside and inside diameters of MWCNT are 5−20 nm, and 2−6 nm, respectively, and their lengths reach up to 10−20 μm. The MWCNT were purified using a mixture of concentrated nitric and sulfuric acids (1:3 in volume ratio) of analytical grade, as reported previously [36]. Polyacrylonitrile (PAN, Mn = 267,000 g/mol) in powder was purchased by Radici group. N,N-dimethyl formamide (DMF) was purchased by Neon Comercial Ltda. with a purity of 99.5%, and used as received.

https://doi.org/10.1016/j.heliyon.2019.e01386

2.2. Electrospun of PAN nanofibers (PF)

PAN was solubilized in DMF under magnetic stirring at 60 °C for 90 min in order to obtain a 6 wt% homogeneous solution. The solution was placed in a glass syringe of 20 mL, and connected to a stainless-steel needle of 0.8 mm in diameter. The electrospun process was carried out inside an acrylic box to have better control of relative humidity. The solution was electrospun over an aluminum foil positioned on a cylindrical collector made of aluminum with diameter and width of 175 mm × 130 mm, respectively. The process was kept at room temperature and a dehumidifier was used to keep the relative humidity in the acrylic box below 60%. The feed rate was set to 1.5 mL/h and the distance of the needle to the target (cylindrical collector) was 8 cm. The solution was electrospun at 13 kV, and the collector rotated at 1000 rpm [26]. The aforementioned parameters of electrospun process allowed obtain preferentially oriented PAN fibers.

2.3. Preparation of buckypapers (BP) and PAN fibers/ buckypapers (BP/PF)

For the preparation of BP samples, firstly, 50 mg of MWCNT were ultrasonically dispersed with the aid of 1 g (1 wt% related to water) of Triton X-100 surfactant, in 100 mL of Milli-Q water, using an ultrasound probe Sonic VCX 750 model (20 kHz, 750 W). The dispersion was centrifuged at 4000 rpm for 30 min. Then, the supernatant of MWCNT suspension was filtrated under vacuum through a nylon membrane with a pore size of 0.45 μm [37].

For BP/PF samples, the dispersion process of MWCNT was the same described for the BP sample preparation. However, after centrifugation step, four layers of PF (45 mm × 45 mm) were stacked over a nylon membrane, as illustrated in Fig. 1a. Then, the supernatant of MWCNT suspension was filtrated under vacuum, as shown in Fig. 1b. Both prepared samples were dried at 80 °C for 15 h, and then washed with acetone and isopropyl alcohol [37]. Fig. 2 summarizes the preparation of BP and BP/PF samples.

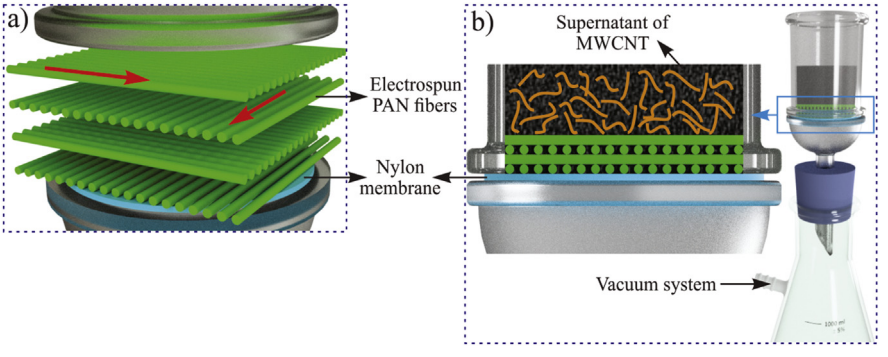

Fig. 1. Schematic illustration for the preparation of BP/PF samples (a) Orientation of PF; (b) Filtration under vacuum of the supernatant of MWCNT suspension.

https://doi.org/10.1016/j.heliyon.2019.e01386

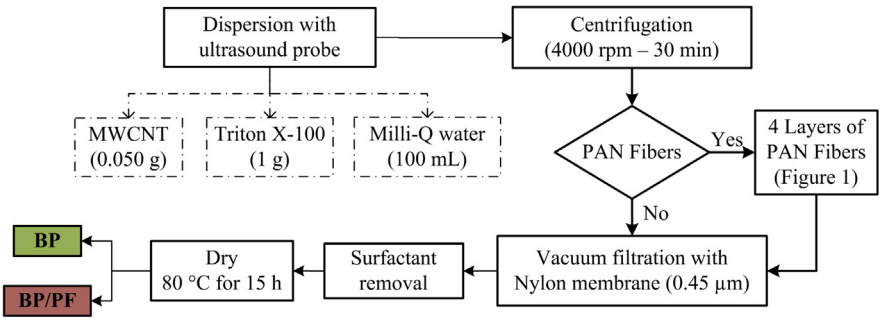

Fig. 2. Summary of BP and BP/PF samples preparation.

2.4. Removal of PF from BP

Firstly, 25 mL of DMF was heated at 60 °C (Corning®, model PC-420D) in a Petri dish. Subsequently, the BP/PF sample was immersed in DMF six times. The time was evaluated in each immersion step: 10 min (BP/PF-10 sample) and 30 min (BP/PF-30 sample), respectively. Both systems (BP/PF-10 and BP/PF-30) were rinsed three times using 25 mL of ethyl alcohol and dried firstly at room temperature for 15 h, and at 80 °C for 2 h Table 1 summarizes the samples prepared in this study.

2.5. Samples characterization

SEM was employed to analyze the cross-section of the samples before and after PAN removal process (FEI Inspect S50 microscopy). SEM images were obtained from secondary electrons, with work distance of 10 mm at 15 kV. Both samples were previously coated with ~5 nm Au layer to avoid charging during electron irradiation.

The residual PAN in BP/PF sample after the PF removal process was investigated by FT-IR using a PerkinElmer Spectrum 2000 equipment, from 3700 to 700 cm^{-1} at a spectral resolution of 4 cm^{-1}. The data were acquired in transmittance mode using KBr pellet technique.

The removal of PF from BP/10 and BP/30 samples were also evaluated by TGA (Netzsch Iris TG F1) at heating rate of 20 °C/min. The temperature was scanned from 200 to 800 °C under inert atmosphere. Measurements were carried out using samples around 5 mg under argon flow rate of 20 mL/min.

Table 1. Samples prepared in this study.

Sample	Time of each immersion in DMF (min)	Description
BP	-	Buckypaper
BP/PF	-	Buckypaper/PAN Fiber
BP/PF-10	10	Buckypaper/PAN Fiber – 10
BP/PF-10	30	Buckypaper/PAN Fiber – 30
PF	-	PAN Fiber

https://doi.org/10.1016/j.heliyon.2019.e01386

The textural properties, surface area and total pore volume of BP, BP/PF-10, and BP/PF-30 samples were determined by a conventional volumetric technique at 77 K using nitrogen. Firstly, all samples were dried under vacuum for 15 h at 80 °C and then they were degassed for 3 h at 80 °C. The analyses were performed on a Quantachrome Nova 4200e equipment. The surface area was calculated by using the Brunauer − Emmett − Teller (BET) method and the total pore volume ($V_{0.98}$) was determined by the amount of nitrogen adsorbed at $P/P_0 = 0.98$.

The crystalline structures of samples were characterized at room temperature by XRD (Rigaku X-ray diffractometer model Ultima IV) operating with Cu Kα radiation ($\lambda = 1.54178$ Å), voltage of 40 kV, and intensity of 30 mA. Multiple detectors (fast detection mode) were used at angular increments of 0.01°, and a scan speed of 10°/min, resulting in a high signal level. Diffractograms were obtained in the angular region of $2\theta = 10-50°$.

The sheet resistance measurements of samples were carried out at room temperature using a four-point probe with the aid of the Universal Probe with RM3000 Test Unit from Jandel Engineering Ltd. with spacing probe S = 1 mm.

High-resolution transmission electron microscopy (HRTEM) was performed on field emission gun FEI Tecnai G2F20 operating with an acceleration voltage of 200 kV. The samples were prepared using carbon electron microscope grids.

3. Results & discussion

Fig. 3 shows PF and the cross-section of BP, BP/PF, and BP/PF-10 samples. Fig. 3a shows preferentially oriented PF (dotted arrows) obtained from the electrospinning process with an average diameter of 318 ± 40 nm. Ramakrishna et al. [27] reported that when the rotation of collector is slow, the fibers deposited will be randomly oriented. As the collector speed increases, more oriented fibers can be obtained. This information is relevant since in Fig. 3a it can be observed some fibers with different directions (continuous arrows). Fig. 3b shows the morphology of BP without PF. In this sample the MWCNT were randomly filtrated and an uniform nanometric network of low porosity along its cross-section is formed. Fig. 3c shows the cross-section of BP/PF before washing with DMF with long PF leaving from the network of MWCNT. These fibers have an average diameter of 343 ± 19 nm. In addition, it can be observed that some MWCNT were deposited on the PF surface. As mentioned earlier in this work, Lopes et al. [18] reported the buckypaper is formed only by MWCNT, showing an intrinsic permeability of 8−10 times smaller than observed for conventional mats based on micrometric glass fibers. This is important information since Fig. 3d shows the cross-section of BP/PF-10 after PF removal process. Both BP/PF-10 and BP/PF-30 samples did not show residual PAN in the cross-section and there was no apparent difference between the two

https://doi.org/10.1016/j.heliyon.2019.e01386

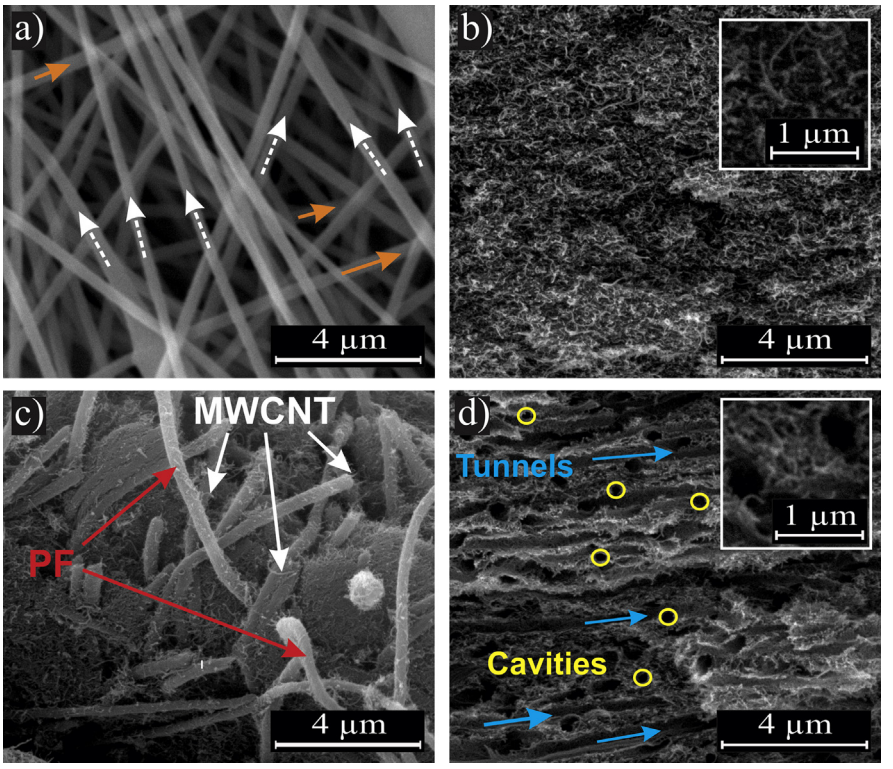

Fig. 3. SEM of (a) PF obtained from electrospinning process; Cross-section of (b) BP; (c) BP/PF before washing with DMF, and (d) BP/PF-10 samples after washing.

samples analyzed by SEM. Tunnels and nanocavities can be easily identified as the structure inherited from PF. Also, the nanocavities have an average diameter of 369 ± 75 nm resulting in a highly porous buckypaper that could facilitate polymer infiltration for high CNT content nanostructured composites.

Fig. 4a shows the FT-IR spectrum for BP, KBr pellet, BP/PF-10, BP/PF-30, BP/PF, and pure PF. The band around of 2243 cm^{-1} can be attributed to nitrile stretching (C≡N) and it is characteristic of PAN [38]. Therefore, the residual PAN in the

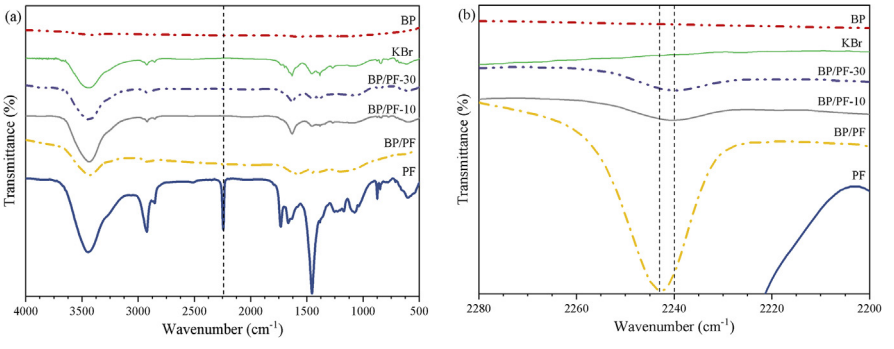

Fig. 4. FT-IR spectra of (a) all samples studied, and (b) Enlargement of FT-IR spectra in the wavenumber range of 2280–2200 cm^{-1}.

https://doi.org/10.1016/j.heliyon.2019.e01386

BP/PF-10 and BP/PF-30 samples was detected through nitrile stretching (2243 cm^{-1}). Fig. 4b shows the enlargement of FT-IR spectra in the wavenumber range of 2280 cm^{-1} to 2200 cm^{-1}, and it can be noted for BP/PF, BP/PF-10, and BP/PF-30 samples the presence of nitrile group. Also, this band was shifted from 2243 cm^{-1} to 2240 cm^{-1}, and it can be associated with PAN dissolution process in DMF, as reported by Wu et al. [39].

Fig. 5 shows the TGA thermograms of BP, PF, BP/PF, BP/PF-10, BP/PF-30 samples. As widely reported in the literature [40, 41, 42], the CNT interact strongly with the oxygen at temperatures above 500 °C leading to their thermal degradation. Therefore, the use of this material under an oxidizing atmosphere should be carried out at temperatures below 500 °C [43, 44]. This information is relevantly important since the BP displays a constant weight loss until 800 °C, and its residual yield was about 92%. Also, as the TGA measurements were carried out in an inert atmosphere, it prevented the oxidation of the MWCNT. Then, the additional weight loss (8%) can be attributed to the degradation of organic groups incorporated on the surface of MWCNT after the functionalization process [45]. The onset temperature for PF starts near to 290 °C, and its loss continues quickly near to 480 °C, presenting a residual mass of ~50% at 800 °C. This behavior is in accordance with other works previously published [26, 46]. The thermal degradation of BP/PF sample starts around 300 °C and ends near 460 °C showing a residual mass of about 82%. In addition, BP/PF-10 and BP/PF-30 samples exhibit a weight-loss around 324 °C with a residual mass of 90% and 88%, respectively. This result is consistent with those previously presented by FT-IR, indicating the residual mass of PAN in the MWCNT network. The highest percentage of weight loss for BP/PF sample compared to BP/PF-10 and BP/PF-30 samples was expected since the BP/PF sample has the PAN fibers without any removal process. This mean that this sample has a higher mass of PAN to be decomposed during the thermal analysis compared to the BP/PF-10 and BP/PF-30 samples. On the other hand, the PF

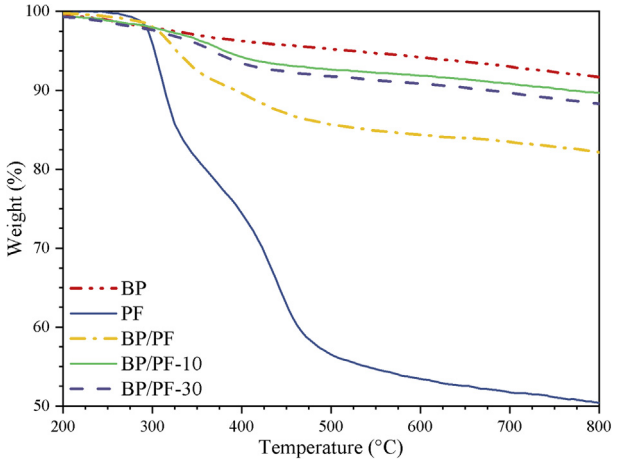

Fig. 5. TGA curves for BP, PF, BP/PF, BP/PF-10, and BP/PF-30 samples.

https://doi.org/10.1016/j.heliyon.2019.e01386

removal process for BP/PF-30 sample presented a bit more amount of PAN in MWCNT network. Since PAN removal process involves temperature (60 °C), and long solubilization times (180 min) it favors the gradual evaporation of DMF, which increases the concentration of the PAN-DMF solution with the consequent reduction of the efficiency of the rinse process [47].

Fig. 6 shows the N_2 adsorption/desorption isotherms for BP, BP/PF-10, and BP/PF-30 systems. The isotherms do not have a well-defined classification in the IUPAC, but basically followed the IV type isotherm, typically for mesoporous materials, associated with pore condensation [48, 49, 50]. Nevertheless, the location and shape of the hysteresis loop show a difference between the BP and other samples after the PAN removal process. BP displays H1 type hysteresis loop, which is characteristic of materials having well-defined cylindrical pores with elevated capillary condensation of N_2 gas in the internal cavity [50]. It can be seen for BP/PF-10 and BP/PF-30 samples the hysteresis loop is next to H3 type, typical of plate-like particle aggregates, which give rise to slit-like pores. In addition, a decrease is in evidence in total pore volume ($V_{0.98}$) from 1.00 cm^3/g to 0.82 cm^3/g, and to 0.78 cm^3/g for BP/PF-10 and BP/PF-30, respectively (Table 2). This behavior suggests possibly a portion of PAN solution is filling the MWCNT, blocking the channel, as previously reported by Sun et al. [47] and Bazilevsky et al. [51]. In addition, the surface area calculated for BP, BP/PF-10 and BP/PF-30 using BET method was 136 m^2/g for all samples, as summarized in Table 2. This indicates that the PAN removal process did not affect the surface area of the samples. Also, the surface area value (136 m^2/g) is slightly lower than reported in other researches [52, 53].

XRD spectra in Fig. 7 shows peaks at 16.9° (200) and 29.8° (020), which correspond to crystal planes of PAN [54, 55], and peaks at 25.6° (002) and 42.9° (100) attributed to the graphite structure of MWCNT [56, 57]. In BP/PF samples the four peaks are easily identified. On the other hand, for the BP/PF-10 and BP/PF-30 systems the

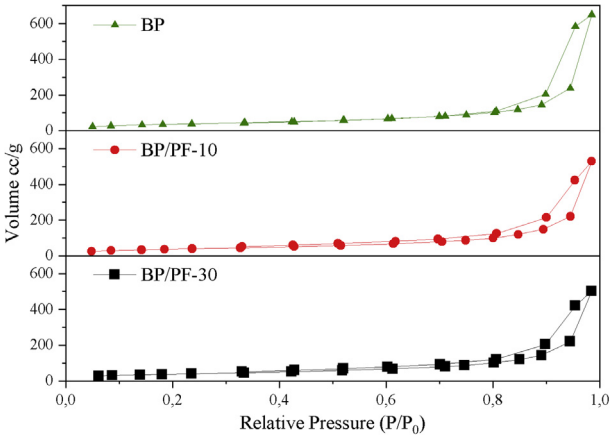

Fig. 6. N_2 adsorption/desorption isotherms for BP, BP/PF-10, and BP/PF-30 samples.

https://doi.org/10.1016/j.heliyon.2019.e01386

Table 2. Textural properties (surface area and $V_{0.98}$), crystallite size (L_{002}) in XRD, and sheet resistance for BP, BP/PF, BP/PF-10, and BP/PF-30 samples.

	BET Surface area (m^2/g)	$V_{0.98}$ (cm^3/g)	L_{002} (nm)	Sheet resistance Ω/square
BP	136	1.00	5.04	6.64 ± 0.43
BP/PF	-	-	4.79	10.35 ± 0.70
BP/PF/10	136	0.82	5.22	124.01 ± 0.10
BP/PF/30	136	0.78	5.19	88.25 ± 0.08

peaks corresponding to PAN were not found. By using the Scherrer equation it was possible to estimate the L_{002} values and the results are summarized in Table 2. As it can be seen, the BP has the crystallite size of 5.04 nm. However, the incorporation of PF into MWCNT network promotes the crystallite size reduction to 4.79 nm. This behavior can be possibly attributed to the inclusion of PF since it creates compression forces in the MWCNT network, which reduces the crystallite size. On the other hand, Sun et al. [47] reported that independently of temperature and time applied during PAN removal process, the tubes always remain with a residual mass of PAN making easy the filling of CNT by polymer since the gradual evaporation of solvent promotes the solution to be even more concentrated with PAN. This information is crucial since both BP/PF-10 and the BP/PF-30 crystallite size increased to 5.22 nm and 5.19 nm, respectively, compared to BP. This behavior can be associated with PF dissolution since a residual mass of PAN is filling in the MWCNT causing stress forces that increase the crystallite size. These results are consistent considering the decreasing in total pore volume presented previously in this work.

The prepared BP has a thickness around 64 μm and a sheet resistance of 6.64 Ω/square. This result is in agreement to that reported by Hussein et al. [58] for

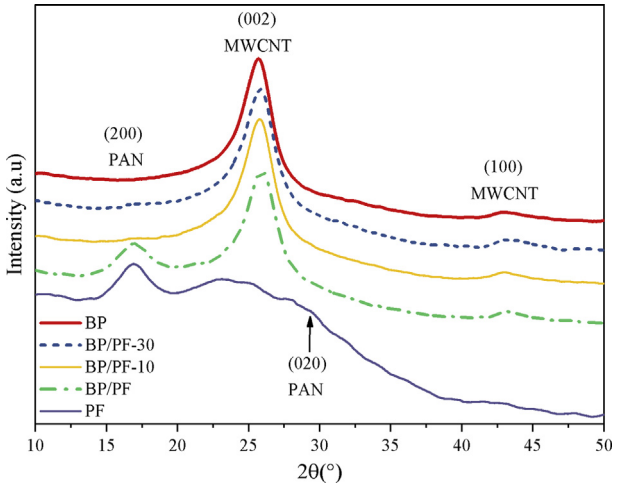

Fig. 7. XRD patterns of BP, PF, BP/PF, BP/PF-10, and BP/PF-30 samples.

https://doi.org/10.1016/j.heliyon.2019.e01386

buckypapers with thickness around 52 μm (8.69 Ω/square) and 77 μm (5.99 Ω/square). After PAN removal process the thickness of BP/PF-10 and BP/PF-30 presented an increase of approximately 42%, and the sheet resistance increased 18.7 times (124.01 Ω/square) and 13.3 times (88.25 Ω/square), respectively. According to Lyons et al. [59], the electrical conductivity of MWCNT buckypaper can be explained by direct contact between the tubes, as shown in Fig. 8a, and Liu et al. [19] defined three types of inter-tube contact that can be found in the CNT, named body-to-body, body-to-end and end-to-end. On the other hand, Sun et al. [47] reported that short times during PAN removal process with DMF revealed that CNT exhibited a rough surface due to the PAN residue on the external surface of the tubes, and for long dissolution periods the external surface of CNT presented an unshaped form as well. Also, in both cases, the solution promoted the filling of CNT by PAN. This information is relevant since if the CNT is possibly filled by the polymer, the increase in the sheet resistance can be attributed to PAN residual mass both on the outer surface and inside the tube for BP/PF-10 and BP/PF-30, reducing the electrical conductivity of the samples. The sheet resistance value determined for BP/PF-30 sample was lower than BP/PF-10 system. This behavior suggests that long dissolution periods allows removing more amount of PAN from the external surface of the MWCNT but not necessarily from the whole MWCNT network, as suggested by TGA. On the other hand, for the BP/PF-10 sample the PAN residue on the surface of MWCNT could reduce even more the inter-tube contact that makes the electrical conduction even more difficult (Fig. 8b). Besides, as shown by SEM image, after the PF removal process, there was the formation of tunnels and cavities in the BP structure that possibly helped the electrical resistivity increase. The sheet resistance for BP, BP/PF, BP/PF-10, and BP/PF-30 are summarized in Table 2.

Fig. 9a shows the HRTEM image of the MWCNT for BP. As can be seen, the MWCNT present a smooth and continuous external surface. On the other hand, Fig. 9b displays the MWCNT for BP/PF-10 with a highly rough surface due to the PAN residual mass deposited on the tube surface. This behavior indicates that short periods of dissolution are not enough to remove effectively the PAN from the MWCNT surface. This observation is consistent with the high increase in sheet

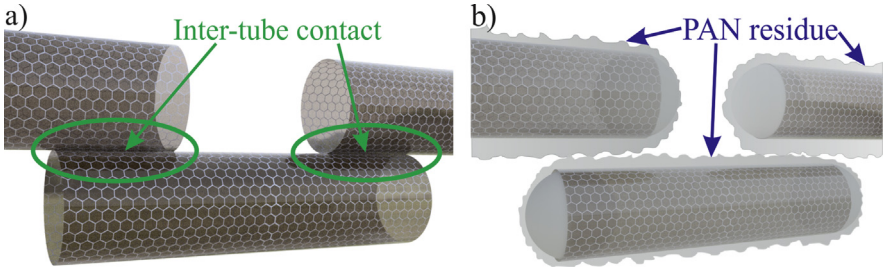

Fig. 8. Graphical representations of inter-tube contact of MWCNT in (a) BP, and (b) PAN residue affecting the inter-tube contact in BP/PF-10.

https://doi.org/10.1016/j.heliyon.2019.e01386

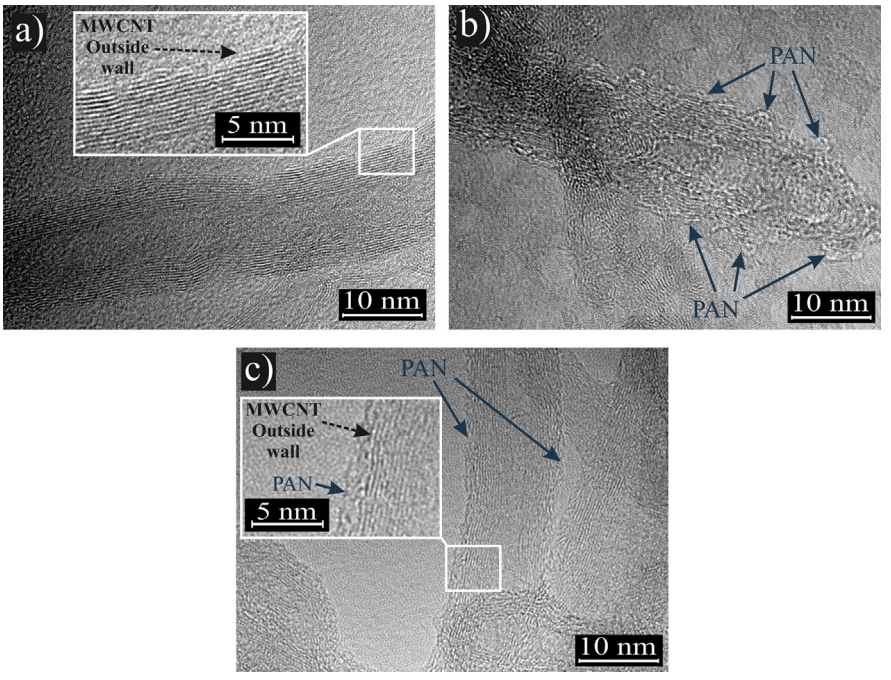

Fig. 9. TEM image of (a) BP; (b) BP/PF-10 and (c) BP/PF-30 samples.

resistance previously presented in this work. Fig. 9c shows the BP/PF-30 sample with a less rough surface of the tube compared to the BP/PF-10 sample. Similar results of roughness were reported by Sun et al. [47]. As discussed earlier, lower roughness can suggest that long dissolution periods can remove more efficiently the PAN from the CNT surface but at the same time, it would possibly favor the filling of the tube, as suggested by the results of TGA, BET, and XRD. Also, less amount of PAN on the MWCNT surface for BP/PF-30 can explain the fact that this sample presented a lower sheet resistance compared to BP/PF-10. This behavior suggests that the inter-tube contact is more PAN free, which makes easy the electrical conduction. More studies need to be carried out to determine the amount of PAN that is filling the MWCNT.

The great advantage of have PAN residual mass in the MWCNT network is the flexibility acquired by the samples, as represented in Fig. 10b, that allows the BP/PF-10

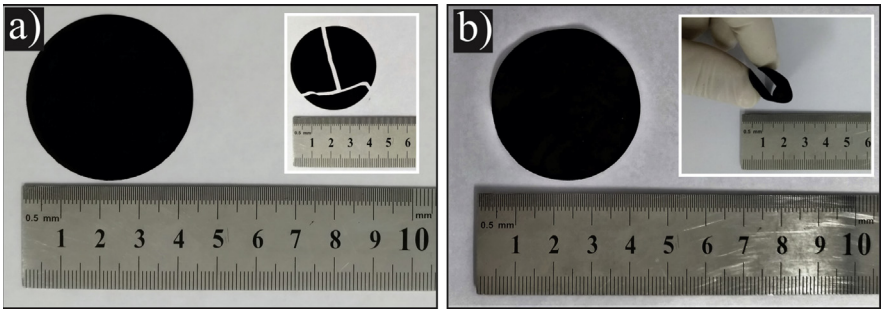

Fig. 10. Difference between flexibilities of (a) BP, and (b) BP/PF-30 samples.

https://doi.org/10.1016/j.heliyon.2019.e01386

and BP/PF-30 systems to be easily bent almost 180° without breaking. This characteristic facilitates the handling of samples compared to the neat BP that presents a fragile behavior (Fig. 10a). The inclusion of PF in the MWCNT network besides to result in a macroporous material, as observed by SEM, also allowed a good flexibility of the buckypaper.

4. Conclusions

Highly porous buckypapers by using PAN nanofibers with an average diameter of 318 nm as sacrificial material were prepared. SEM images did not show differences between samples prepared with 10 min and 30 min PAN removal time, respectively.

FT-IR showed a band around 2243 cm^{-1}, which corresponds to nitrile group (C≡N) characteristic of PAN, indicating the presence of PAN residual in BP/PF-10 and BP/PF-30 samples. Besides, residue of PAN was also evidenced by TGA, which show differences of 2% and 4% in the weight loss, respectively, compared to the neat BP. Moreover, XRD showed that the PF inclusion into BP reduced the L_{002} from 5.04 nm to 4.79 nm possibly by compression forces in the MWCNT network. On the other hand, when PAN is removed from BP the L_{002} presented an increase to 5.22 nm and 5.19 nm for BP/PF-10 and BP/PF-30, respectively. Also, the total pore volume decreased from 1.00 cm^3/g to 0.82 cm^3/g and to 0.78 cm^3/g for BP/PF-10 and BP/PF-30 samples, respectively. HRTEM showed that for short periods of PAN removal (10 min) the CNT showed a highly rough shape due to the presence of PAN residue on the tube surfaces. On the other hand, in long periods (30 min), the tube surface is less rough suggesting a more efficient dissolution of PAN from BP. In addition, it suggested a possible filling of the tubes by PAN since with increasing time the solvent is evaporated and the solution is enriched with PAN. The sheet resistance presented an increase from 6.64 Ω/square (BP) to 124.01 Ω/square (BP/PF 10), and 88.25 Ω/square (BP/PF 30). This increase in sheet resistance is attributed to PAN residue in the inter-tube contact and inside the tube that reduced the electrical conductivity of samples.

Declarations

Author contribution statement

Jefersson A Rojas: Conceived and designed the experiments; Performed the experiments; Analyzed and interpreted the data; Wrote the paper.

Laura A. Ardila, Milton F. Diniz, Maraísa Gonçalves: Analyzed and interpreted the data.

https://doi.org/10.1016/j.heliyon.2019.e01386

Bruno Ribeiro: Contributed reagents, materials, analysis tools or data; Wrote the paper.

Mirabel C. Rezende: Conceived and designed the experiments; Contributed reagents, materials, analysis tools or data; Wrote the paper.

Funding statement

This work was supported by the Brazilian Funding Institutions FAPESP (Fundação de Amparo à Pesquisa do Estado de São Paulo) (2017/04740-0), CAPES (Coordenação de Aperfeiçoamento de Pessoal de Nível Superior), CNPq (Conselho Nacional de Desenvolvimento Científico e Tecnológico) (303287/2013-6).

Competing interest statement

The authors declare no conflict of interest.

Additional information

No additional information is available for this paper.

Acknowledgements

The authors thank the Laboratory of Structural Characterization of the Federal University of São Carlos (LCE/DEMa/UFSCar) for the general facilities, and the Technological Institute of Aeronautics (ITA).

References

[1] B.G. Demczyk, Y.M. Wang, J. Cumings, M. Hetman, W. Han, A. Zettl, R.O. Ritchie, Direct mechanical measurement of the tensile strength and elastic modulus of multiwalled carbon nanotubes, Mater. Sci. Eng. A. 334 (2002) 173−178.

[2] J.Y. Huang, S. Chen, Z.F. Ren, Z. Wang, K. Kempa, M.J. Naughton, G. Chen, M.S. Dresselhaus, Enhanced ductile behavior of tensile-elongated individual double-walled and triple-walled carbon nanotubes at high temperatures, Phys. Rev. Lett. 98 (2007) 185501.

[3] H. Dai, E.W. Wong, C.M. Lieber, Probing electrical transport in nanomaterials: conductivity of individual carbon nanotubes, Science 272 (1996) 523−526.

[4] J. Hone, M. Whitney, C. Piskoti, A. Zettl, Thermal conductivity of single-walled carbon nanotubes, Phys. Rev. B 59 (1999) R2514.

https://doi.org/10.1016/j.heliyon.2019.e01386

[5] Z. Wang, Z. Liang, B. Wang, C. Zhang, L. Kramer, Processing and property investigation of single-walled carbon nanotube (SWNT) buckypaper/epoxy resin matrix nanocomposites, Compos. Part A Appl. Sci. Manuf. 35 (2004) 1225−1232.

[6] A.M. Díez-Pascual, J. Guan, B. Simard, M.A. Gómez-Fatou, Poly(phenylene sulphide) and poly(ether ether ketone) composites reinforced with single-walled carbon nanotube buckypaper: II - mechanical properties, electrical and thermal conductivity, Compos. Part A Appl. Sci. Manuf. 43 (2012) 1007−1015.

[7] M.N. Disfani, S. Jafari, Assessment of intertube interactions in different functionalized multiwalled carbon nanotubes incorporated in a phenoxy resin, Polym. Eng. Sci. 53 (2013) 168−175.

[8] P.-C. Ma, N.A. Siddiqui, G. Marom, J.-K. Kim, Dispersion and functionalization of carbon nanotubes for polymer-based nanocomposites: a review, Compos. Part A Appl. Sci. Manuf. 41 (2010) 1345−1367.

[9] A.M. Díez-Pascual, M. Naffakh, J.M. González-Domínguez, A. Ansón, Y. Martínez-Rubi, M.T. Martínez, B. Simard, M.A. Gómez, High performance PEEK/carbon nanotube composites compatibilized with polysulfones-I. Structure and thermal properties, Carbon N. Y. 48 (2010) 3485−3499.

[10] S. Zhang, B.E. Leonhardt, N. Nguyen, A. Oluwalowo, C. Jolowsky, A. Hao, R. Liang, J.G. Park, Roll-to-roll continuous carbon nanotube sheets with high electrical conductivity, RSC Adv. 8 (2018) 12692−12700.

[11] X. Yang, J. Lee, L. Yuan, S.-R. Chae, V.K. Peterson, A.I. Minett, Y. Yin, A.T. Harris, Removal of natural organic matter in water using functionalised carbon nanotube buckypaper, Carbon N. Y. 59 (2013) 160−166.

[12] J. Zhang, D. Jiang, Influence of geometries of multi-walled carbon nanotubes on the pore structures of Buckypaper, Compos. Part A Appl. Sci. Manuf. 43 (2012) 469−474.

[13] S. Bose, R. a. Khare, P. Moldenaers, Assessing the strengths and weaknesses of various types of pre-treatments of carbon nanotubes on the properties of polymer/carbon nanotubes composites: a critical review, Polymer (Guildf) 51 (2010) 975−993.

[14] A.M. Díez-Pascual, J. Guan, B. Simard, M.A. Gómez-Fatou, Poly (phenylene sulphide) and poly (ether ether ketone) composites reinforced with single-walled carbon nanotube buckypaper: I - structure, thermal stability and crystallization behaviour, Compos. Part A Appl. Sci. Manuf. 43 (2012) 997−1006.

https://doi.org/10.1016/j.heliyon.2019.e01386

[15] S.M. Cooper, H.F. Chuang, M. Cinke, B.A. Cruden, M. Meyyappan, Gas permeability of a buckypaper membrane, Nano Lett. 3 (2003) 189−192.

[16] W. Zhu, J.P. Zheng, R. Liang, B. Wang, C. Zhang, S. Walsh, G. Au, E.J. Plichta, Highly-efficient buckypaper-based electrodes for PEMFC, Prot. Exch. Membr. Fuel Cells 8 (Pts 1 2) (2008) 16., 1615−1626＼r2188.

[17] U. Vohrer, I. Kolaric, M.H. Haque, S. Roth, U. Detlaff-Weglikowska, Carbon nanotube sheets for the use as artificial muscles, Carbon N. Y. 42 (2004) 1159−1164.

[18] P.E. Lopes, F. van Hattum, C.M.C. Pereira, P.J.R.O. Nóvoa, S. Forero, F. Hepp, L. Pambaguian, High CNT content composites with CNT Buckypaper and epoxy resin matrix: impregnation behaviour composite production and characterization, Compos. Struct. 92 (2010) 1291−1298.

[19] L. Liu, Q. Yang, J. Shen, Correlation between porosity and electrical-mechanical properties of carbon nanotube buckypaper with various porosities, J. Nanomater. 2015 (2015).

[20] Á. Kukovecz, R. Smajda, Z. Kónya, I. Kiricsi, Controlling the pore diameter distribution of multi-wall carbon nanotube buckypapers, Carbon N. Y. 45 (2007) 1696−1698.

[21] L. Dumée, K. Sears, J. Schütz, N. Finn, M. Duke, S. Gray, A preliminary study on the effect of macro cavities formation on properties of carbon nanotube bucky-paper composites, Materials (Basel) 4 (2010) 553−561.

[22] R.K. Das, B. Liu, J.R. Reynolds, A.G. Rinzler, V. Gaines, Engineered macroporosity in single-wall carbon nanotube films, Nano Lett. 9 (2009) 677−683.

[23] M.G. McKee, G.L. Wilkes, R.H. Colby, T.E. Long, Correlations of solution rheology with electrospun fiber formation of linear and branched polyesters, Macromolecules 37 (2004) 1760−1767.

[24] T. Jarusuwannapoom, W. Hongrojjanawiwat, S. Jitjaicham, L. Wannatong, M. Nithitanakul, C. Pattamaprom, P. Koombhongse, R. Rangkupan, P. Supaphol, Effect of solvents on electro-spinnability of polystyrene solutions and morphological appearance of resulting electrospun polystyrene fibers, Eur. Polym. J. 41 (2005) 409−421.

[25] J.R. Kim, S.W. Choi, S.M. Jo, W.S. Lee, B.C. Kim, Characterization and properties of P(VdF-HFP)-Based fibrous polymer electrolyte membrane prepared by electrospinning, J. Electrochem. Soc. 152 (2005) A295.

[26] M. Santos de Oliveira Junior, B.V. Manzolli Rodrigues, J.S. Marcuzzo, L.M. Guerrini, M.R. Baldan, M.C. Rezende, A statistical approach to evaluate

 https://doi.org/10.1016/j.heliyon.2019.e01386

the oxidative process of electrospun polyacrylonitrile ultrathin fibers, J. Appl. Polym. Sci. 134 (2017) 1−10.

[27] S. Ramakrishna, K. Fujihara, W.-E. Teo, T.-C. Lim, Z. Ma, An Introduction to Electrospinning and Nanofibers, World Scientific, 2005.

[28] S.Y. Gu, J. Ren, G.J. Vancso, Process optimization and empirical modeling for electrospun polyacrylonitrile (PAN) nanofiber precursor of carbon nanofibers, Eur. Polym. J. 41 (2005) 2559−2568.

[29] J.B. De Oliveira, L.M. Guerrini, S.S. Oishi, L.R. De Oliveira Hein, L. Dos Santos Conejo, M.C. Rezende, E.C. Botelho, Carbon nanofibers obtained from electrospinning process, Mater. Res. Express 5 (2018).

[30] Z. yu Fan, Y. li Zhao, X. yue Zhu, Y. Luo, M. wu Shen, X. yang Shi, Folic acid modified electrospun poly(vinyl alcohol)/polyethyleneimine nanofibers for cancer cell capture applications, Chinese J. Polym. Sci. (English Ed.) 34 (2016) 755−765.

[31] R. Al-Attabi, L.F. Dumée, J.A. Schütz, Y. Morsi, Pore engineering towards highly efficient electrospun nanofibrous membranes for aerosol particle removal, Sci. Total Environ. 625 (2018) 706−715.

[32] R. Al-Attabi, L.F. Dumée, L. Kong, J.A. Schütz, Y. Morsi, High efficiency poly(acrylonitrile) electrospun nanofiber membranes for airborne nanomaterials filtration, Adv. Eng. Mater. 20 (2018) 1−10.

[33] F.O. Agyemang, G.M. Tomboc, S. Kwofie, H. Kim, Electrospun carbon nanofiber-carbon nanotubes coated polyaniline composites with improved electrochemical properties for supercapacitors, Electrochim. Acta 259 (2018) 1110−1119.

[34] T.-D. Lu, B.-Z. Chen, J. Wang, T.-Z. Jia, X.-L. Cao, Y. Wang, W. Xing, C.H. Lau, S.-P. Sun, Electrospun nanofiber substrates that enhance polar solvent separation from organic compounds in thin-film composites, J. Mater. Chem. A (2018).

[35] B. Sun, Y.Z. Long, Z.J. Chen, S.L. Liu, H. Di Zhang, J.C. Zhang, W.P. Han, Recent advances in flexible and stretchable electronic devices via electrospinning, J. Mater. Chem. C. 2 (2014) 1209−1219.

[36] L.A. Ardila Rodriguez, D.N. Travessa, Core/shell structure of TiO_2 -coated MWCNTs for thermal protection for high-temperature processing of metal matrix composites, Ann. Mater. Sci. Eng. 2018 (2018).

[37] J.A. Rojas, L.A. Ardila-Rodríguez, M.F. Diniz, M. Gonçalves, B. Ribeiro, M.C. Rezende, Optimization of Triton X-100 removal and ultrasound probe

https://doi.org/10.1016/j.heliyon.2019.e01386

parameters in the preparation of multiwalled carbon nanotube buckypaper, Mater. Des. 166 (2019) 107612.

[38] S. Li, X. Yue, Y. Jing, S. Bai, Z. Dai, Fabrication of zonal thiol-functionalized silica nanofibers for removal of heavy metal ions from wastewater, Colloids Surfaces A Physicochem. Eng. Asp. 380 (2011) 229−233.

[39] Q.-Y. Wu, X.-N. Chen, L.-S. Wan, Z.-K. Xu, Interactions between polyacrylonitrile and solvents: density functional theory study and two-dimensional infrared correlation analysis, J. Phys. Chem. B 116 (2012) 8321−8330.

[40] H. Marsh, I.A.S. Edwards, R. Menendez, B. Rand, S. West, A.J. Hosty, K. Kuo, B. McEnaney, T. Mays, D.J. Johnson, J.W. Patrick, D.E. Clarke, J.C. Crelling, R.J.B.T. Gray, Introduction to Carbon Science, Butterworth-Heinemann, 1989.

[41] K.R. DEVI, G. Rohini, RAO, carbon carbon composites: an overview, Def. Sci. J. 43 (2013) 369−383.

[42] E. Savage, Carbon-Carbon Composites, Springer Netherlands, 1993.

[43] P.M. Ajayan, S. Lijima, Capillarity-induced filling of carbon nanotubes, Nature 361 (1993) 333.

[44] Z.P. Wu, J.N. Wang, Preparation of large-area double-walled carbon nanotube films and application as film heater, Phys. E Low-Dimens. Syst. Nanostruct. 42 (2009) 77−81.

[45] V. Datsyuk, M. Kalyva, K. Papagelis, J. Parthenios, D. Tasis, A. Siokou, I. Kallitsis, C. Galiotis, Chemical oxidation of multiwalled carbon nanotubes, Carbon N. Y. 46 (2008) 833−840.

[46] M. Suzuki, C.A. Wilkie, The thermal degradation of acrylonitrile-butadiene-styrene terpolymei as studied by TGA/FTIR, Polym. Degrad. Stabil. 47 (1995) 217−221.

[47] V. Chan, K. Sun, A. Yarin, C.M. Megaridis, Intercalation of Poly-acrylonitrile (PAN) into carbon nanotubes, J. Undergrad. Res. Univ. Illinois Chicago. 52 (2007).

[48] H. Chu, Z. Zhang, Y. Liu, J. Leng, Self-heating fiber reinforced polymer composite using meso/macropore carbon nanotube paper and its application in deicing, Carbon N. Y. 66 (2014) 154−163.

[49] K.S.W. Sing, Reporting physisorption data for gas/solid systems with special reference to the determination of surface area and porosity (Recommendations 1984), Pure Appl. Chem. 57 (1985) 603−619.

https://doi.org/10.1016/j.heliyon.2019.e01386

[50] B. Gao, C. Peng, G.Z. Chen, G. Li Puma, Photo-electro-catalysis enhancement on carbon nanotubes/titanium dioxide (CNTs/TiO2) composite prepared by a novel surfactant wrapping sol-gel method, Appl. Catal. B Environ. 85 (2008) 17–23.

[51] A.V. Bazilevsky, K. Sun, A.L. Yarin, C.M. Megaridis, Selective intercalation of polymers in carbon nanotubes, Langmuir 23 (2007) 7451–7455.

[52] G.Q. Zhang, J.P. Zheng, R. Liang, C. Zhang, B. Wang, M. Hendrickson, E.J. Plichta, Lithium–air batteries using SWNT/CNF buckypapers as air electrodes, J. Electrochem. Soc. 157 (2010) A953–A956.

[53] J.-H. Han, H. Zhang, M.-J. Chen, G.-R. Wang, Z. Zhang, CNT buckypaper/thermoplastic polyurethane composites with enhanced stiffness, strength and toughness, Compos. Sci. Technol. 103 (2014) 63–71.

[54] H. Hou, J.J. Gc, J. Zeng, Q. Li, D.H. Reneker, A. Greiner, S.Z.D. Cheng, Electrospun polyacrylonitrile nanofibers containing a high concentration of well-aligned multiwall carbon nanotubes, Chem. Mater. 17 (2005) 967–973.

[55] Y. Liu, H.G. Chae, S. Kumar, Gel-spun carbon nanotubes/polyacrylonitrile composite fibers. Part I: effect of carbon nanotubes on stabilization, Carbon N. Y. 49 (2011) 4466–4476.

[56] X.J. Fan, X. Li, Preparation and magnetic properties of multiwalled carbon nanotubes decorated by Fe_3O_4 nanoparticles, Xinxing Tan Cailiao/New Carbon Mater. 27 (2012) 111–116.

[57] L. Kong, X. Lu, W. Zhang, Facile synthesis of multifunctional multiwalled carbon nanotubes/Fe_3O_4 nanoparticles/polyaniline composite nanotubes, J. Solid State Chem. 181 (2008) 628–636.

[58] L. Hussein, G. Urban, M. Krüger, Fabrication and characterization of buckypaper-based nanostructured electrodes as a novel material for biofuel cell applications, Phys. Chem. Chem. Phys. 13 (2011) 5831–5839.

[59] P.E. Lyons, S. De, F. Blighe, V. Nicolosi, L.F.C. Pereira, M.S. Ferreira, J.N. Coleman, The relationship between network morphology and conductivity in nanotube films, J. Appl. Phys. 104 (2008).

https://doi.org/10.1016/j.heliyon.2019.e01386